**MATSAS: A Small Angle Scattering Computer Tool for Porous Systems** 

Amirsaman Rezaeyan a\*, Vitaliy Pipich b and Andreas Busch a

<sup>a</sup> Lyell Centre, Institute of GeoEnergy Engineering, Heriot-Watt University, Research Avenue South,

Edinburgh, EH14 4AS, Scotland

<sup>b</sup> Heinz Maier-Leibnitz Zentrum (MLZ), Forschungszentrum Jülich GmbH, Jülich Centre for Neutron

Science (JCNS), Lichtenbergstrasse 1, Garching, 85748, Germany

Correspondence email: ar104@hw.ac.uk; amirsaman.rezaeyan@gmail.com

Synopsis MATSAS analyses small angle scattering of neutrons and X-rays data obtained from porous

systems. MATSAS delivers a full suite of pore characterisations including specific surface area,

porosity, pore size distribution, and fractal dimensions.

**Abstract** MATSAS is a script-based MATLAB® program for analysis of small angle scattering

(SAS) of neutrons and X-rays data obtained from various facilities. The program has primarily been

developed for sedimentary rock samples but is equally applicable for other porous media. MATSAS

imports raw SAS data from XLS(X) or CSV files, combines small angle scattering and very small angle

scattering data, subtracts the sample background, and displays the processed scattering curves in log-

log plots. MATSAS uses the polydisperse spherical (PDSP) model to obtain structural information of

scatterers (scattering objects); for a porous system, results include specific surface area (SSA), porosity

(Φ), and differential and logarithmic differential pore area/volume distributions. In addition, pore and

surface fractal dimensions ( $D_p$  and  $D_s$ , respectively) are obtained from the scattering profiles. The

program package allows simultaneous and rapid analysis of a batch of samples (countless); results are

then exported to XLSX and CSV files with separate spreadsheets for individual samples. MATSAS is

the first SAS program that delivers a full suite of pore characterisations for sedimentary rocks.

MATSAS is an open-source package, which is freely available at GitHub (https://github.com/matsas-

software/MATSAS).

Keywords: MATSAS; Small angle scattering; polydisperse spherical model; porous media.

#### 1. Introduction

Small-angle scattering (SAS) of neutrons and X-rays (SANS and SAXS) is widely used to nondestructively study the low-resolution structure of natural and engineered systems, including sedimentary rocks, biological macromolecules, composite nanomaterials, or polymers on the length scales between Angstroms and microns in a single or combined experiment (Feigin & Svergun, 1987, Binder et al., 2000, Zemb & Lindner, 2002, Radlinski, 2006, Borsali & Pecora, 2008, Anovitz & Cole, 2015, Melnichenko, 2015, Fritzsche et al., 2016). Advances in SAS instrumentation such as neutron radiation and high-flux X-ray synchrotron beamlines have significantly increased the use of SANS and SAXS experiments (Melnichenko, 2015, Zemb & Lindner, 2002, Heenan et al., 1997). Despite the availability of these technologies, modern instruments provide high quality data in timeor space-resolved experiments or measurements under various physical and chemical conditions, such as temperature, pressure, humidity, etc (Konarev et al., 2006, Schrank et al., 2020). Obtained over past decades, theoretical and methodological developments have allowed the retrieval of structural information from SAS patterns to address questions revolving around the size, shape, distribution, and orientation of scattering objects) (Konarev et al., 2006, Petoukhov et al., 2012). Neutron and X-ray scattering techniques complement each other, however, they are different in the charge, energy, and the interaction with matter, which make each of them subject to its own experimentation type and/or sample type (Binder et al., 2000, Zemb & Lindner, 2002, Melnichenko, 2015). Figure 1 illustrates a pinhole SAS experiment. Neutrons or X-rays are collimated and monochromatised towards the sample inside which a neutron or photon is elastically scattered from its wave vector  $k_{\theta}$ into the state with wave vector k under the scattering angle 2 $\theta$ . The magnitude of a wave vector relates to wave number, which is  $|\mathbf{k}| = |\mathbf{k}_0| = k = 2\pi/\lambda$  for the elastic scattering, where  $\lambda$  is the neutron or X-ray wavelength. The intensity of scattered radiation dI is therefore measured in direction k as a function of the momentum transfer (the convention  $\mathbf{s} = |\mathbf{k} - \mathbf{k}_0|$ ) or the so-called scattering vector  $\mathbf{Q}$ . The magnitude of the scattering vector is given by  $Q = 4\pi \sin\theta/\lambda$  in which follows that  $\mathbf{Q} = 2\pi \mathbf{s}$ where  $s = 2\sin\theta/\lambda$ .(Radlinski, 2006, Melnichenko, 2015).

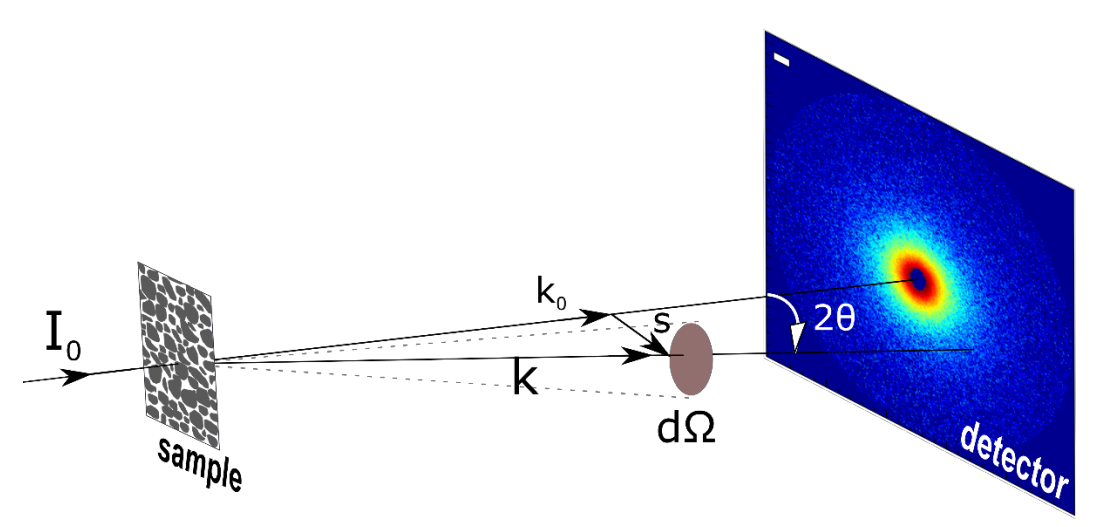


**Figure 1** The schematic principle of a SAS experiment.

The incident flux of the scattering objects is denoted by  $\Phi_0$ , i.e.,  $\Phi_0 = I_0/A$ , where  $I_0$  is the incident intensity (neutrons/X-rays per second) and A is the beam cross sectional area at the sample position (**Error! Reference source not found.**) (Radlinski, 2006). The scattered intensity monitored in the solid angle element  $d\Omega$  targeted by the scattering vector Q can be expressed as

$$dI \propto \Phi_0 \frac{d\Sigma}{d\Omega} d\Omega \tag{1}$$

where  $d\Sigma$  is the elemental scattering cross section. The quantity  $d\Sigma/d\Omega$  is called the differential cross section of scattering (Radlinski, 2006). The aim of SAS experiments is to determine volume-averaged information on the spatial distribution of scattering length density (neutrons) or the electron density (X-rays) in the sample from the measured  $d\Sigma/d\Omega$  as a function of scattering vector Q;  $\frac{d\Sigma}{d\Omega}(Q)$  or I(Q) (Melnichenko, 2015).

For a wide range of substances, the SAS data for hard and soft matter can generally be interpreted accurately using a two-phase approximation (Melnichenko, 2015). In this approximation, the scattering volume is viewed as comprised of supra-molecular-size phases, each characterised by one of two possible values of the physical property that provides the scattering contrast ( $\Delta \rho^*$ ). For instance, for porous media these two phases are the solid matrix (phase 1) and the pore space (phase 2), respectively (Radlinski, 2006). The two-phase approximation is a simplification inherent in the SAS method and has been implicitly or explicitly employed for many years. As such, the general expression of the scattering cross section can be expressed as:

$$I(Q) = NV_p^2 (\rho_1^* - \rho_2^*)^2 P(Q)S(Q) + B$$
(2)

where N is the number density of scatterers  $N_p$  per unit volume,  $V_p$  is the volume of scatterers, and  $\rho_1^*$  and  $\rho_2^*$  are the scattering length/electron density of phase 1 and phase 2, respectively. B is the sample background, accounting for scattering in the high Q-limit. The large-Q background originates from (1) a Q-independent incoherent scattering caused by hydrogen atoms in organic matter and/or water, and (2) a Q-dependent coherent scattering resulting from microscopic inhomogeneities (e.g. small pores in the rock matrix (Bahadur *et al.*, 2015, Blach *et al.*, 2020)). P(Q) is the so-called form factor that describes the size and shape of the scatterer. There are analytical expressions for the form factor for simple geometrical objects like spheres, cylinders, discs, parallelepipeds (Melnichenko, 2015). S(Q) is called the structure factor that contains information about spatial distribution of the scatterers. The structure factor represents the modification of the intensity due to the spatial correlation of the scatterers (Fritzsche *et al.*, 2016) where the positions of scatterers are frozen in time and space in solid porous materials (Melnichenko, 2015). In soft matter systems, the interaction potential between

scatterers is also taken into consideration (Melnichenko, 2015). Form and structure factors need to be specified to determine the structural information of scattering curves.

Several SAS programs have been developed in different laboratories that consider various data processing and manipulation methods, fitting models, and form and structure factors to characterise the structure of scatterers (Table 1). Recognising the increasing application of SAS data to analyse the pore structure of sedimentary rocks, especially low permeability rocks such as coal and mudrocks or gas shales (Radlinski, Ioannidis, *et al.*, 2004, Radlinski, Mastalerz, *et al.*, 2004, Radlinski *et al.*, 2009, Mares *et al.*, 2012, Clarkson *et al.*, 2012, Mastalerz *et al.*, 2012, Melnichenko *et al.*, 2012, Bahadur *et al.*, 2014, Anovitz *et al.*, 2015, Bahadur *et al.*, 2015, Leu *et al.*, 2016, Busch *et al.*, 2017, Anovitz & Cole, 2018, Busch *et al.*, 2018, Sakurovs *et al.*, 2018, Vishal *et al.*, 2019, Blach *et al.*, 2020), we developed the program package MATSAS. It allows analysing data obtained from small angle and very small angle scattering of neutrons and X-rays (VSANS, SANS, WAXS, USAXS, and SAXS).

**Table 1** Common SAS programs and their capabilities and applicabilities.

SAS Program	Capabilities	Applicability	Reference		
FIT2D	2D image data reduction/manipulation and peak fitting	-	(Hammersley, 1995)		
BerSANS	Data acquisition/reduction	-	(Keiderling, 1997)		
DALAI_GA	Ab initio shape determination	Biological systems	(Chacón et al., 1998)		
FISH	Peak analysis and parametric fitting using various form and structure factors	-	(Heenan, 1999)		
SAX3D	Ab initio shape determination	Biological systems	(Walther et al., 2000)		
SAXS/WAXS software system	Data acquisition/reduction	-	(Homan et al., 2001)		
GRASP	Data acquisition/reduction	-	(Dewhurst, 2002)		
SAXSANA	Data reduction, Q determination, data conversion, data correction, analysis of time-resolved data, and data extrapolation	Biological systems	Hiragi <i>et al.</i> (2003)		
PRINSAS*	Fitting of 1D curve using spherical form factor for a polydisperse scattering system	Porous systems	(Hinde, 2004)		
ATSAS	Data reduction, data processing and 3D modelling	Biological systems	(Konarev <i>et al.</i> , 2006, Petoukhov <i>et al.</i> , 2012)		

DAMMIF	Ab-initio shape determination for disordered systems and solutions	Nanostructures	(Franke & Svergun, 2009)	
IRENA*	Plotting SAS data, merging of two overlapping data sets, and fitting form and structural models to data from contrast variation experiments	A wide range of systems	(Ilavsky & Jemian, 2009)	
BioXTAS RAW	Isotropic SAXS data reduction, primary data analysis, and the calculations of the pair-distance distribution functions	Biological systems	(Nielsen et al., 2009)	
SCATTER	2D data analysis	Nano- and mesoscale oriented structures	(Forster et al., 2010)	
SAAF	SANS data analysis using a set of standard models	Polymers	(Zhao, 2011)	
SASTBX	Data reduction, model reconstruction, model refinement, and shape retrieval	Biological systems	(Liu et al., 2012)	
SASET	1D and 2D data analysis and fitting of data using scattering models and anisotropy methods	Anisotropic structures	(Muthig et al., 2013)	
MolScat and SAFIR	Modelling of three-dimensional macromolecular structures	Biological systems	(Hofmann & Whitten, 2014)	
SASfit	Reduction of oversampled data sets, confidence assessment of the optimised model parameters, and availability of custom user-provided models	Polymers	(Bressler et al., 2015)	
BioXTAS RAW	Averaging, subtraction and analysis of radius of gyration and molecular weight, calculation of inverse Fourier transforms and envelopes, processing of inline size-exclusion chromatography coupled SAXS data, and data deconvolution	Biological systems	(Hopkins et al., 2017)	
QtiSAS/QtiKWS*	Graphical visualisation, reduction, analysis, and fit of data using various scattering models	A wide range of systems	https://www.qtisas.com/	
SASview*	Data reduction, manipulation, and analysis using several form and structure	A wide range of systems	http://www.sasview.org/	

MATSAS analyses data from pinhole geometry, time of flight (TOF) and Bonse-Hart machines and was tested using data acquired from FRM-II (Research Reactor Munich II, Garching, Germany) and ORNL (Oak Ridge National Laboratory, Tennessee, USA) (Rezaeyan, Pipich, et al., 2019a, b, 2019, Seemann et al., 2019). MATSAS does post-processing of data obtained from research facilities, assuming that initial corrections for sample thickness, transmission, detector sensitivity, instrument backgrounds, multiple scattering, and noise have been done using the instrument specific settings at the facility itself, providing data in absolute units (Hinde, 2004, Melnichenko, 2015). MATSAS is primarily oriented towards the structural analysis of sedimentary rocks using a polydisperse spherical (PDSP) model. The MATSAS software is constantly refined to broaden the functionality, making it applicable for isotropic and partially ordered objects such as biological nanoparticle systems, colloidal solutions, and polymers in solution and bulk. It is an open source computer tool for academic users, which is freely available on GitHub (https://github.com/matsas-software/MATSAS). Besides, opensource access reflects transparency in the fundamental assumptions and solving approaches employed in the program and allows third parties to interface their in-house programs with the data analysis framework of the program (Liu et al., 2012) and help accelerating its development. In this paper, we summarise the main components of MATSAS and its development framework.

## 2. Program Overview

MATSAS features a script-based package in MATLAB® (The MathWorks Inc., Cambridge, UK), which integrates computation and visualisation in an easy-to-use environment. The MATSAS program is a versatile computer tool allowing both users and developers to add additional tools and develop specific novel applications. The flexible user-friendly framework of MATSAS to basic routines, such as intensity calculation or model alignment, allows anyone with basic programming skills to improve or adapt MATSAS to better reflect user-specific needs. Furthermore, the current version of the package includes the PDSP model to analyse SAS data in terms of theoretical intensity computation, f(r) probability function of pore size distribution, and model refinement. The PDSP model is the method commonly used for SAS analysis of a polydisperse system of randomly oriented independently scattering particles, which is ubiquitous for fractal microstructures (e.g., sedimentary rocks) as well as other porous systems (Radlinski, Ioannidis, *et al.*, 2004), provided that the particle-shape distribution is independent of the distribution of particle dimensions in the polydisperse system (Schmidt, 1982). The script-based MATSAS allows tuning parameters for more features of each routine. Nevertheless, use of the MATSAS program is divided into three steps: (1) the pre-processing

<sup>\*</sup> PRINSAS, IRENA, QtiSAS, and SASview are commonly used for analysis of SAS data obtained from porous systems featuring a wide range of pore sizes.

of raw or facility post-corrected SAS and very-small-angle scattering (VSAS) data as well as physical information, (2) the processing of the imported information to produce I(Q) versus Q curves, combine the SAS and VSAS curves, and fit the PDSP model, and (3) the post-processing to display and export structural information obtained from the samples being analysed. Figure 2 illustrates main components of the present version of MATSAS.

The detailed instructions to use the package is available on GitHub. Supporting information and command descriptions are embedded in each module. Errors and bugs can be invoked when no parameter or incorrect data is given to the command. We developed the package in Windows and recommend running it in Windows, Mac, or Linux, with any Intel or AMD x 86-64 processor with four logical cores and AVX2 instruction set support, as a minimum. Although the program runs satisfactorily without a specific graphics card, a hardware accelerated graphics card supporting OpenGL 3.3 with 1GB GPU memory is recommended as displaying figures and generating Microsoft Excel worksheets require more background processing.

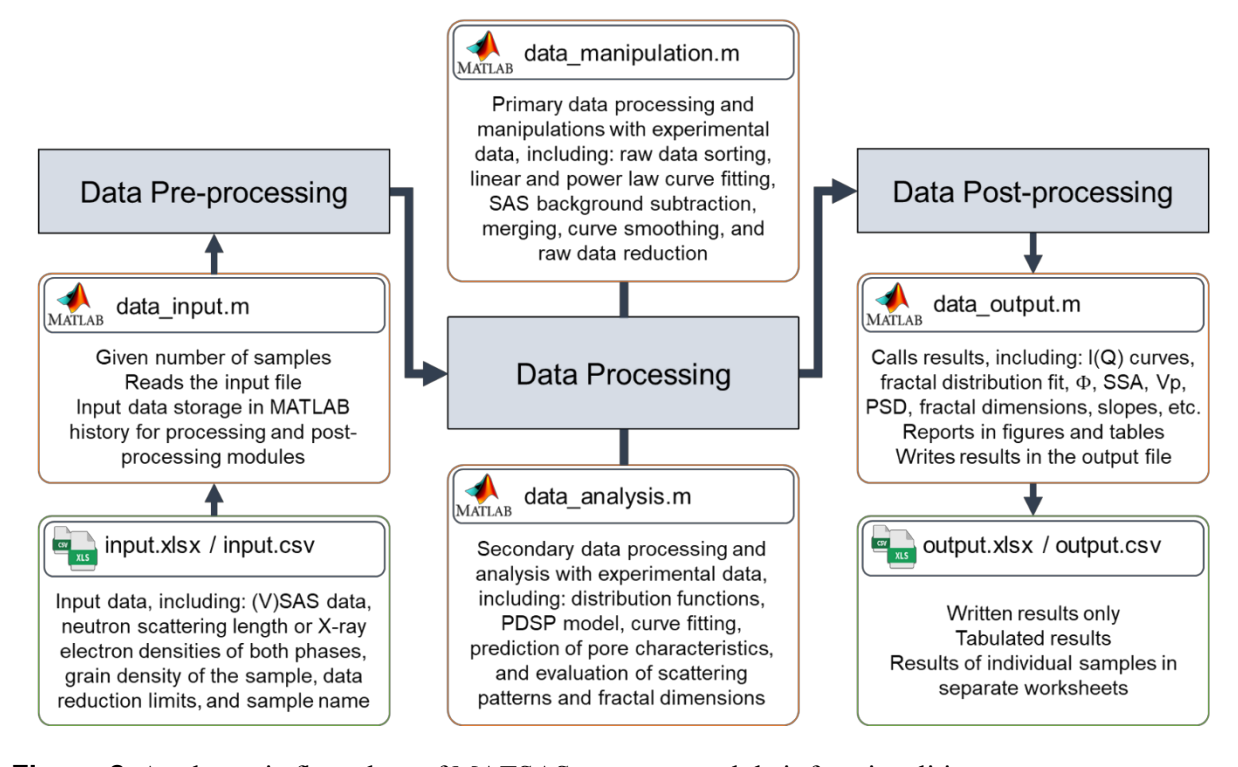


Figure 2 A schematic flow chart of MATSAS programs and their functionalities.

### 3. Data Pre-processing

The data pre-processing module is composed of two compartments: (A) data are prepared in Microsoft Excel spreadsheet or CSV files-\*.xls(x) or \*.csv files, including (V)SAS data, neutron scattering length densities or X-ray electron densities of phases 1 and 2 (e.g. rock matrix and pore), grain density of the sample, data reduction limits (optional), and sample name, and (B) MATLAB data\_input.m file reads and stores the imported data for the next step. MATSAS allows users to run a

batch of samples. The units in the input files can be converted between different unit systems (between nm<sup>-1</sup> and Å<sup>-1</sup> for Q, for instance) by changing appropriate codes. The range(s) of data points can be adjusted for each data set individually or simultaneously for selected groups of files.

# 4. Data Processing

The data processing module is used to manipulate and analyse the information imported. The primary data processing script is developed to manipulate scattering curves. The data\_manipulation.m file carries on multiple tasks, including: I(Q) data sorting, curve fittings, background subtraction, curves merging, curve smoothing, and raw data reduction. The secondary data processing script file is designed in data\_analysis.m to analyse I(Q)-Q curves and produce structural information. An arbitrary size distribution is created in the first place and the PDSP model is then fitted to the processed scattering curve. Pore characteristics are predicted and fractal dimensions (including pore fractal dimension,  $D_p$ , surface fractal dimension,  $D_s$ , and general fractal dimension,  $D_f$ ) are evaluated from the fit in this module.

## 4.1. Data Manipulation

The program data\_manipulation.m is a data processing module encompassing major SAS data processing steps for isotropic systems, from scattering curves merging to background reduction. This program performs manipulations with one-dimensional data sets and calls other analysis and fitting programs via user defined or built-in function files. The SAS data are possibly collected at different sample-to-detector distances. Once data of several experimental curves are combined for one specific instrument (e.g., SANS), they may not be sorted, which leads to numerical problems in further analysis. Data sorting is therefore carried out in the data manipulation package using a built-in function. Provided that SAS data consists of two scattering profiles obtained from two different instruments (e.g., VSANS and SANS), MATSAS allows users to merge the two curves using a least-squares fitting in the overlapping range as illustrated for sample in Figure 3Error! Reference source not found. The SAS curve is the basis onto which the VSAS curve is rebinned. The large-Q background is subtracted using Equation (3):

$$\frac{d\Sigma}{d\Omega}(Q) = A Q^{-a} + \left[ \frac{d\Sigma}{d\Omega}(Q) \right]_{inc} \tag{3}$$

in case the scattering varies with  $Q^{-a}$  in the high Q-limit before plateau (Melnichenko, 2015). The value of the background  $\left[\frac{d\Sigma}{d\Omega}(Q)\right]_{inc}$  is determined from a linear plot of Equation (4):

$$Q^{a} \frac{d\Sigma}{d\Omega}(Q) = A + Q^{a} \left[ \frac{d\Sigma}{d\Omega}(Q) \right]_{inc} \tag{4}$$

where  $\left[\frac{d\Sigma}{d\Omega}(Q)\right]_{inc}$  is the slope and A is the intercept (Melnichenko, 2015). Figure 3 shows the background subtraction in the high Q-limit for a range that users can manually change in the program. A noise removal operation is embedded to remove the sparse data around the beam stop or detector edge. The raw data reduction whose cut-off limits are determined in the data input files is carried out as well. Two data smoothing operations are included in the package that can be employed to make a smooth scattering profile for further structural analysis. Fractal dimensions and slope are determined here. For all operations, the propagation of uncertainty is performed using standard equations (Bevington & Robinson, 2003). A MATLAB plotting operation displays currently active scattering profiles in logarithmic-logarithmic scale. An advanced plotting option included in the plot permits users to change the plotting range, zoom factor, etc. The data manipulation file contains an output section, where the result of each operation can be further used in subsequent data analysis. Information about the operation (type of operation, section names, functions, weights, ranges of points used, etc.) is written in the package in green that allows modifying or changing lines if needed.

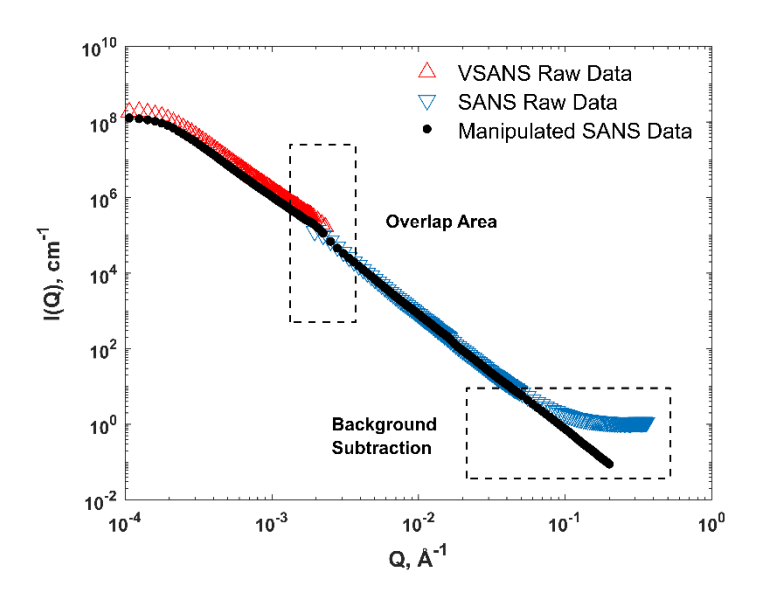


**Figure 3** SANS data manipulated and processed on an arbitrary mudrock sample. Red, blue, and black curves are the scattering profiles from the VSANS instrument, from the SANS instrument, and the net scattering after manipulation (merging, background subtraction, and smoothing), respectively.

# 4.2. Data Analysis

The data analysis program calculates the intensity of small angle scattering from a polydisperse system of scatterers (Porod, 1951, 1952, Guinier & Fournet, 1955). The intensity is expressed in terms of fractal distribution of scatterers, also called the probability density of the pore size distribution f(r), for a greater numerical stability (Ilavsky & Jemian, 2009). SAS curves from sedimentary rocks are usually linear on a log-log scale, particularly in the large-Q region, which reflects fractal behaviour (Melnichenko, 2015). Scattering from a fractal surface is equivalent to the scattering from a system of

polydisperse spherical scatterers (PDSP) (Schmidt, 1982), with a number size distribution (the number of spheres with radii between R and R+dR) given by

$$f(r)dR \sim R^{-(1+D_f)}dR \tag{5}$$

where  $D_f$  is the fractal dimension determined from the slope of the power-law scattering (Melnichenko, 2015). Practically, the distribution described in Equation (5) and ranging from  $R_{min} \le R \le R_{max}$  shows fractal behaviour between the upper and lower cut-off parameters. f(r) is expressed as  $f(r) = \frac{D_f}{R_{min}^{-D_f} - R_{max}^{-D_f}} R^{-(1+D_f)}$ , which is valid for  $R_{max} > R_{min} > 0$  and  $D_f \in (-1, \infty)$  where  $D_f = 6 + slope$ . Scattering from a PDSP featured sample has a linear region with a similar slope  $-(1 + D_f)$  and is described by (Radlinski, Ioannidis,  $et\ al.$ , 2004):

$$I(Q) = \int_{R_{min}}^{R_{max}} (\rho_1^* - \rho_2^*)^2 N f(r) V^2 P(Q, r) dr$$
 (6)

where  $V \equiv V(r) = \frac{4}{3}\pi r^3$  is the volume of a sphere of radius r (volume of scatterer). In addition, P(Q,r) is the form factor of a sphere of radius r due to (Guinier & Fournet, 1955):

$$P(Q,r) = \left[ 3 \frac{\sin(Q,r) - Qr \cos(Q,r)}{O^3 r^3} \right]^2$$
 (7)

N is the total number of scatterers, which is related to the number size distribution as N(r) = N f(r). N(r) is expressed as:

$$N(r) = \frac{\Phi}{\bar{V}(r)} f(r) = \frac{IQ_0}{(\rho_1^* - \rho_2^*)^2} \frac{1}{\bar{V}^2(r)}$$
(8)

where  $IQ_0 = f(r)(R_{max} - R_{min})\Phi \frac{(\rho_1^* - \rho_2^*)^2}{\bar{V}(r)}$  is the scattering intensity at Q = 0 and  $\bar{V}(r) = 0$ 

 $\int_{R_{min}}^{R_{max}} V(r) f(r) dr$  is the average volume of scatterers (Radlinski *et al.*, 2002). Similar to Ilavsky and Jemian (2009), MATSAS calculates Equation (6) throughout the integration over a continuous size distribution with a summation over a discrete size histogram:

$$I(Q) = \sum_{i} (\rho_{1i}^* - \rho_{2i}^*)^2 \sum_{i,j} N_i f_i(r_{i,j}) V_i(r_{i,j})^2 P_i(Q_i, r_{i,j}) \Delta r_{i,j}$$
(9)

where the subscript *i* represents different scattering sizes and the subscript *j* describes bins in the size distribution.  $\Delta r_{i,j}$  is the width of bin j; each scattering size has its own binning index *i,j*. *r* is the dimension of the scatterer (radius for spheres) that has limits  $r_{max_i}$  and  $r_{min_i}$ . Radius *r* is calculated using  $R = 2\pi/Q$ , which is R = 2.5/Q in the fractal distribution (Radlinski *et al.*, 2000).

MATSAS uses an arbitrary size distribution that is used to model the scattering volume distribution  $V^2(r) P(Q, r)$  as well as to determine f(r). Users can change the theoretical ranges of the various size distributions in the data analysis program. Numerical calculations call limits on the range of

dimension  $(r_{min} \text{ and } r_{max})$ , cut-off limits  $(R_{min} \text{ and } R_{max})$ , and number of bins  $(N_{bin})$ . This method results in a natural logarithmic stepping in dimension and uses three parameters  $-R_{min}$ ,  $R_{max}$ , and  $N_{bin}$ . The centre of the first  $(r_{i,1})$  and the last  $(r_{i,N_{bin}})$  bins are  $R_{max}$  and  $R_{min}$ , respectively and extra fractional volumes are discarded for both bins: the volume associated with  $r_{min_{i,1}} - r_{i,1}$  and  $r_{i,N_{bin}} - r_{max_{i,N_{bin}}}$  for the first and last bins, respectively. The width of bins are equal by selecting associated dimensions at regular increments of the cumulative distribution (Ilavsky & Jemian, 2009), leading to  $\log(\Delta) = \frac{\log(R_{max}) - \log(R_{min})}{N_{bin}}$ . However, the numerical operation of the data\_analysis.m file, requires  $r_{min_{i,j}}$ ,  $r_{i,j}$ ,  $r_{max_{i,j}}$ ,  $f_i(r_{i,j})$ , and  $IQ_{0i}$  to fit the PDSP model in Equation (6) to the measured I(Q) curve. The fitting procedure employs f(r) and  $IQ_0$  as fitting parameters for each iteration to attain the match where the summation of square errors (SSQ) tends to a minimum (Hinde, 2004). Furthermore, to decrease the computation time due to numerical integration, we found an analytical solution for the scattering volume distribution:

$$\int_{R_{min}}^{R_{max}} V^{2} P(Q,r) dr = \sum_{i,j} \frac{1}{Q_{i}^{7}} \left( 16\pi^{2} \left( -\frac{5}{4} \sin(Q_{i} r_{i,j}) \cos(Q_{i} r_{i,j}) + \frac{3}{2} Q_{i} r_{i,j} \cos(Q_{i} r_{i,j})^{2} + Q_{i}^{2} r_{i,j}^{2} \left( \frac{1}{2} \sin(Q_{i} r_{i,j}) \cos(Q_{i} r_{i,j}) + \frac{1}{2} Q_{i} r_{i,j} \right) - \frac{1}{4} Q_{i} r_{i,j} - \frac{1}{3} Q_{i}^{3} r_{i,j}^{3} \right) \Delta r_{i,j} \tag{10}$$

that transforms Equation (9) into:

$$I(Q) = \sum_{i} (\rho_{1i}^{*} - \rho_{2i}^{*})^{2} \sum_{i,j} N_{i} f_{i}(r_{i,j}) \frac{1}{Q_{i}^{7}} \left( 16\pi^{2} \left( -\frac{5}{4} \sin(Q_{i}r_{i,j}) \cos(Q_{i}r_{i,j}) + \frac{3}{2} Q_{i}r_{i,j} \cos(Q_{i}r_{i,j})^{2} + Q_{i}^{2}r_{i,j}^{2} \left( \frac{1}{2} \sin(Q_{i}r_{i,j}) \cos(Q_{i}r_{i,j}) + \frac{1}{2} Q_{i}r_{i,j} \right) - \frac{1}{4} Q_{i}r_{i,j} - \frac{1}{3} Q_{i}^{3} r_{i,j}^{3} \right) \Delta r_{i,j}$$

$$(11)$$

MATSAS simplifies the intensity calculation by substituting Equation (8) into Equation (11), leading to:

$$I(Q) = \sum_{i,j} IQ_{0i} f_i(r_{i,j}) \bar{V}_i^{-2}(r_{i,j}) \frac{1}{Q_i^{7}} \left( 16\pi^2 \left( -\frac{5}{4} \sin(Q_i r_{i,j}) \cos(Q_i r_{i,j}) + \frac{3}{2} Q_i r_{i,j} \cos(Q_i r_{i,j})^2 + Q_i^2 r_{i,j}^2 \left( \frac{1}{2} \sin(Q_i r_{i,j}) \cos(Q_i r_{i,j}) + \frac{1}{2} Q_i r_{i,j} \right) - \frac{1}{4} Q_i r_{i,j} - \frac{1}{3} Q_i^3 r_{i,j}^3 \right) \Delta r_{i,j}$$

$$(12)$$

Once the match is reached, the data analysis program yields structural characteristics of scatterers using fitted f(r) and  $IQ_0$  values. The specific surface area (SSA) of scatterers is obtained following Hinde (2004):

$$SSA = \frac{1}{\rho_g(\rho_1^* - \rho_2^*)^2} \sum_k \frac{4}{3} \pi \, IQ_{0_k} \, f(r_k) \, \bar{V}^{-2}(r_k) \, \Delta r_k \tag{13}$$

where the subscript k represents bins in the size distribution. The volume fraction of scatterers per unit volume ( $\Phi$ ) is calculated from Equation (8), which results in:

$$\Phi = \frac{1}{(\rho_1^* - \rho_2^*)^2} \sum_k IQ_{0_k} \bar{V}(r_k) \bar{V}^{-2}(r_k)$$
(14)

and the total volume of scatterers  $(V_n)$  is obtained by:

$$V_p = \frac{1}{\rho_g} \sum_k \frac{\Phi(r_k)}{1 - \Phi(r_k)} \tag{15}$$

where the subscript k represents bins in the size distribution. Differential (dV/dr or dA/dr) and logarithmic differential scatterer size distributions (dV/dlogr or dA/dlogr) are calculated cumulatively (Meyer & Klobes, 1999).

The scattering intensity decays as  $Q^{-m}$  with different power-law exponents m; it indicates that the power-law exponent (m) is related to the dimensionality of the pore as understood based on the concept of fractality (Mandelbrot, 1983). For a pore fractal scatterer, therefore,  $D_p = m$ , with values  $1 < D_p < 3$  and for a surface fractal  $D_s = 6 - m$  with values  $2 \le D_s \le 3$  (Bale & Schmidt, 1984). Furthermore, the scattering at different length scales indicates the Guinier, the mass/pore fractal, the surface fractal, and Porod regions that suggest each fractal region is limited to a specific range of scattering vectors (Fritzsche  $et\ al.$ , 2016). Therefore, for sedimentary rocks  $D_p$  and  $D_s$  are geared to the range of  $0.0003 - 0.003\ cm^{-1}$  and  $0.003 - 0.03\ cm^{-1}$ , respectively.  $D_f$  is additionally included to reflect on the fractality of the full pore system over the entire scattering vector e.g.,  $0.0003 - 0.03\ cm^{-1}$  in sedimentary rocks (Rezaeyan, Pipich,  $et\ al.$ , 2019a, b, 2019). These ranges are can be changed by the user.

For demonstration purposes, we tested the analysis operations on SANS and VSANS data obtained from 3 rock samples (Opalinus Clay) using batch mode. Opalinus Clay is a Jurassic mudrock that was obtained from the Mont Terri Underground Laboratory in Switzerland and has been described in detail previously (Busch *et al.*, 2017). Figure 4-A shows the PDSP modelled I(Q) curves and the measured I(Q) curves after two iterations of the fitting operation. The first iteration starts with an initial guess for f(r) and  $IQ_0$ , which is obtained from the slope of the scattering curves and the Guinier and Fournet (1955) approximation, respectively. SSQ tends to a minimum after the second iteration; two iterations are recommended for most rock samples (Hinde, 2004). Figure 4-B shows f(r) after two iterations on a log-log scale. f(r) levels off at scatterer sizes  $> 2 \mu$ m because the scattering intensity of large scatterers are smeared, possibly due to instrument artefacts at the edge of the detector. The error sensitivity, expressed as  $dSSQ/dlog(IQ_0)$ , relates SSQ to the number of iterations (Figure 4-C). The  $dSSQ/dlog(IQ_0)$  varies around zero for all scatterer sizes. However, as illustrated in Figure 4-C this can deviate where the fit is rather poor for large scatterer sizes (3 < log(D) < 3.5) due to different instrument resolutions or noise within overlap areas. SSQ magnifies

when the number of iterations exceeds 2, resulting in an attenuation of f(r). Nevertheless, we recommend attaining a smooth f(r) if the optimum fit requires a larger number of iterations for a specific sample. Chi squared tolerance can be used for the fit when the number of iterations is unpreferable for users. Furthermore, we tested the PDSP model on 3 Polydimethylsiloxane (PDMS) polymers with the volume fractions 0.128, 0.25 and 0.5 in toluene to demonstrate the applicability of the fitting operation for a non-power law nanostructure in solution (Figure 4- D through F). Figure 4-F displays the numerical flexibility of the fitting procedure after 20 iterations.

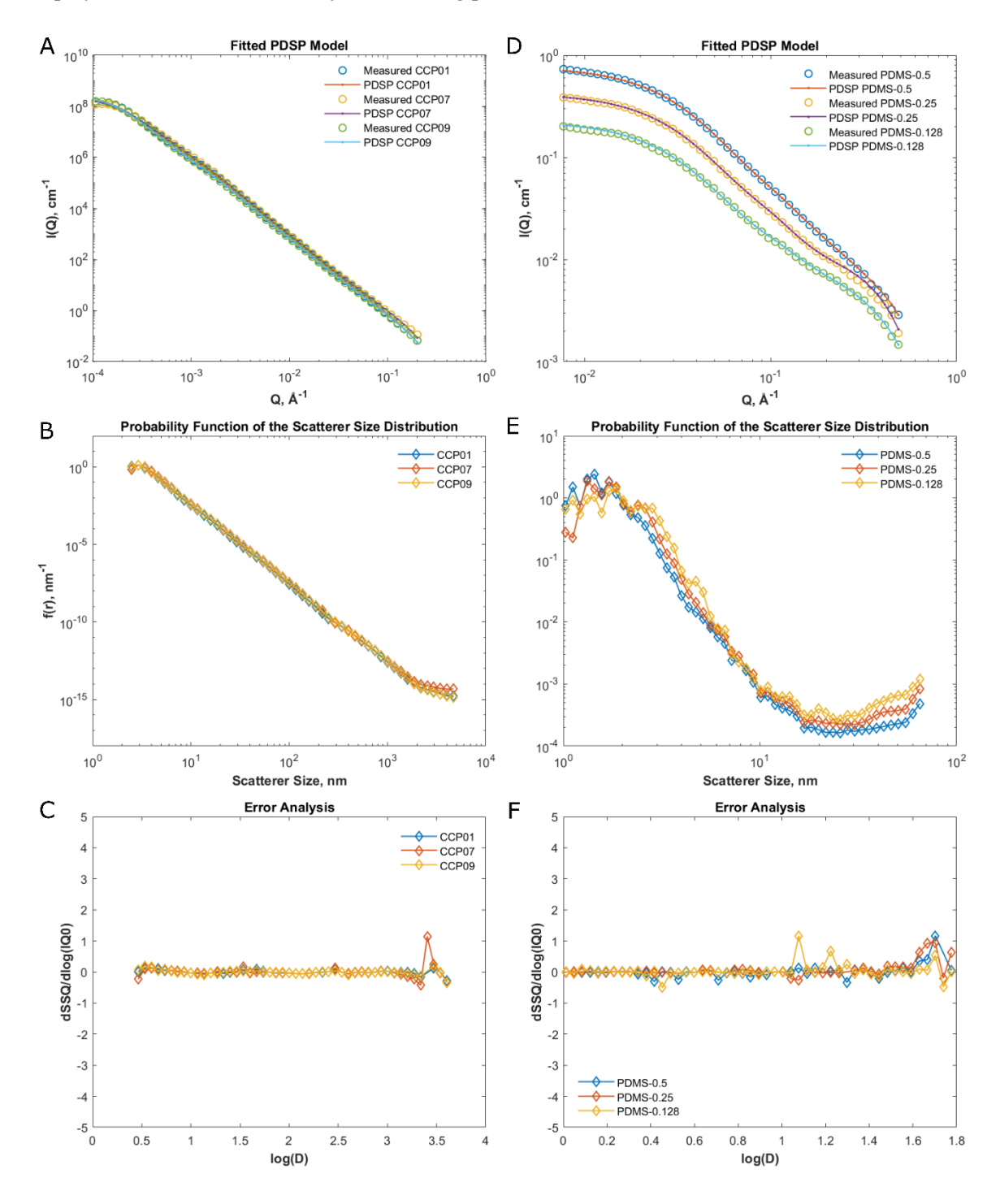


**Figure 4** PDSP model applied to SANS data obtained from 3 rock samples (Opalinus Clay) and 3 Polydimethylsiloxane (PDMS) polymers of the volume fractions 0.128, 0.25, and 0.5 in toluene. Rock samples: (A) Measured I(Q) curves after manipulation and I(Q) curves obtained from PDSP model; (B) probability functions of the pore size distribution f(r); (C) error sensitivity  $dSSQ/dlog(IQ_0)$  obtained after 2 iterations. PDMS samples: (D) the fitted PDSP model; (E) probability functions of the scatterer size distribution f(r); (F) error sensitivity obtained after 20 iterations.

# 5. Data Post-processing

The data post-processing module is made of two compartments, including data\_output.m in MATLAB® and the results reported in figures and tabulated files. The data\_output.m file calls the results of individual samples, reports results in figures and tables in the MATLAB Command Window and writes the results in output.xlsx. The results include measured, processed, and predicted scattering curves, fractal distribution fit ( $f_r$ ), specific surface area (SSA), porosity ( $\Phi$ ), pore volume ( $V_p$ ), pore size distribution (PSD) by pore volume or pore area, fractal dimensions, the slope of scattering curves, pore characteristics divided in macro-, meso-, and micropores, and background subtraction values. Some of results are shown in Figure 5 and Table 2. The results of individual samples are produced and saved in figure formats (\*.tiff and \*.emf), Excel spreadsheets, and CSV files for users for further specific analyses. It should be noted that the results are usable if raw SAS data are provided in absolute unit, otherwise users must report pore characteristics in arbitrary unit.

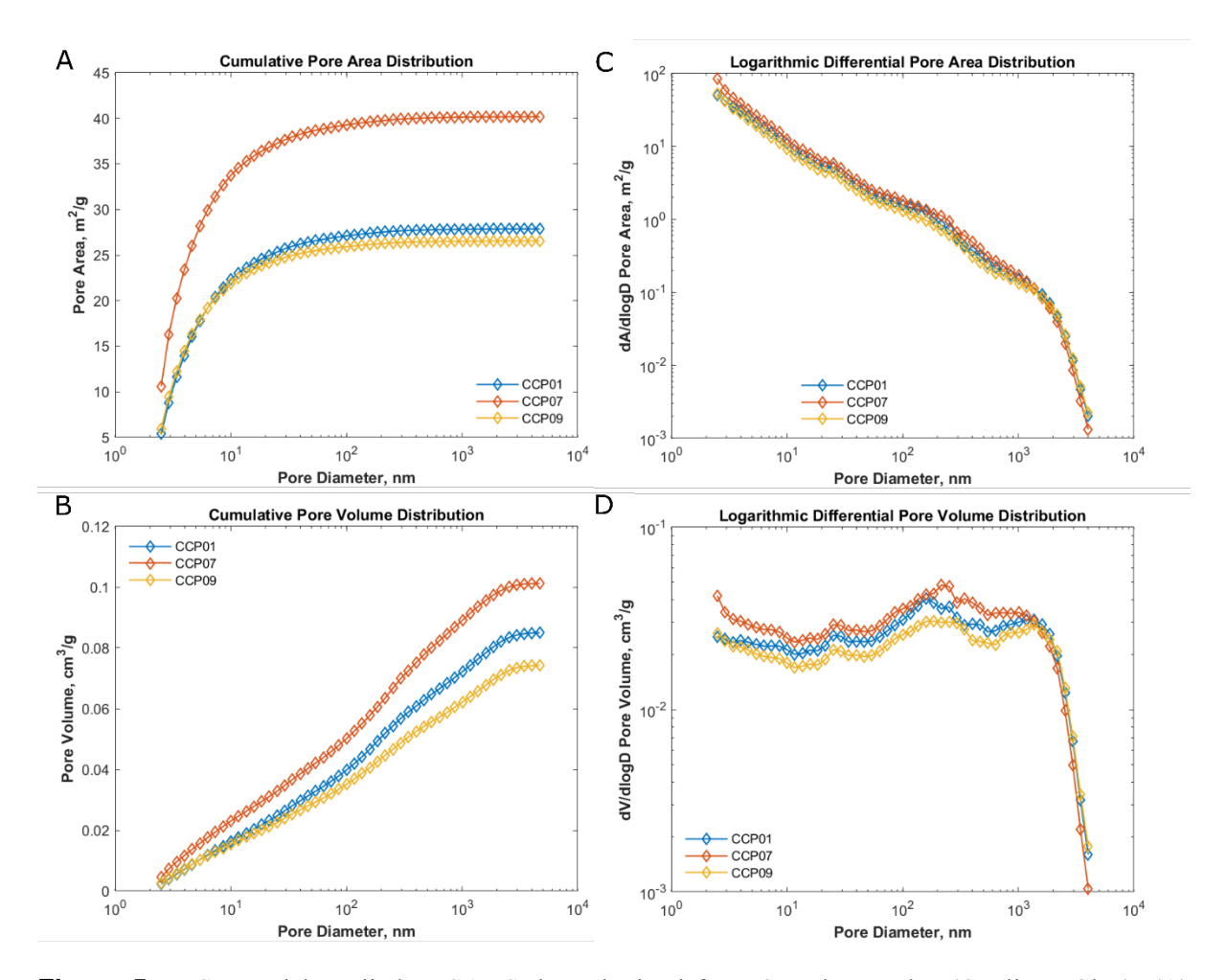


**Figure 5** PDSP model applied to SANS data obtained from 3 rock samples (Opalinus Clay). (A) Cumulative pore area distribution; (B) logarithmic differential pore area distribution; (C) cumulative pore volume distribution; (D) logarithmic differential pore volume distribution.

**Table 2** Slope (m), fractal dimensions (D), incoherent background (I<sub>BG</sub>), and pore characteristics evaluated by MATSAS from the SANS data of 3 rock samples.

Sample	m	$D_{\mathrm{f}}$	Ds	Dp	I <sub>BG</sub> v <sub>SAS</sub>	I <sub>BG SAS</sub>	SSA	SSA <sub>macro</sub>	SSA <sub>meso</sub>
ID									
	-	-	-	-	cm <sup>-1</sup>	cm <sup>-1</sup>	$m^2/g$	$m^2/g$	$m^2/g$
CCP01	-3.06	2.94	2.88	2.84	15317	1.15	31.6	1.4	30.2
CCP07	-3.05	2.95	2.88	2.76	7032	1.23	44.8	1.6	43.1
CCP09	-3.07	2.93	2.88	2.86	14818	0.92	29.6	1.2	28.5
Table <b>2</b> (continued).									
$V_p$	V <sub>macro</sub>	V <sub>meso</sub>	Ф	$\Phi_{ ext{macro}}$	$\Phi_{ ext{meso}}$	SSQ	Chi <sup>2</sup>	<u> </u>	
cm <sup>3</sup> /g	cm <sup>3</sup> /g	cm <sup>3</sup> /g	%	%	%	-			

0.0880	0.0541	0.0339	23.7	14.6	9.1	0.01	0.003
0.1036	0.0601	0.0435	28.0	16.3	11.8	0.09	0.006
0.0773	0.0472	0.0301	21.1	12.9	8.2	0.01	0.005

The subscripts meso and macro represent properties in meso- and macropore sizes, respectively.

#### 6. Conclusion

MATSAS encompasses a set of modules allowing for a full analysis of (V)SANS and (V)SAXS data from porous systems e.g., sedimentary rocks. MATSAS is written in MATLAB® that combines a desktop environment tuned for data processing and structural analyses with pre- and post-processing modules. The pre-processing module is used to import data from Microsoft Excel spreadsheets or CSV files into MATLAB®. The main module performs data manipulation and analysis in which I(Q)-Q curves are processed and the PDSP model is fitted to produce the structural information of porous systems. The post-processing module displays results in forms of tables and figures and exports them in Microsoft Excel spreadsheets or CSV files. MATSAS is the first SAS program that provides a full suite of pore characterisations. The programs included in MATSAS are publicly available on GitHub (https://github.com/matsas-software/MATSAS) for academic users.

Acknowledgements SANS and VSANS measurements on the rock samples tested here were performed at KWS-1 and KWS-3 instruments of the Jülich Centre for Neutron Science (JCNS) at Heinz Maier-Leibnitz Zentrum (MLZ) in Garching, Germany. We are very grateful for the beam time obtained. We also thank Masoud Ghaderi Zefreh of the University of Edinburgh for assisting with MATLAB programs as well as Gernot Rother of the Oak Ridge National Laboratory, Artem Feoktystov of the Forschungszentrum Jülich GmbH, and Lester Barnsley of the Australian Synchrotron for testing and reporting on MATSAS.

#### References

- Anovitz, L. M. & Cole, D. R. (2015). Reviews in Mineralogy and Geochemistry 80, 61-164.
- Anovitz, L. M. & Cole, D. R. (2018). *Geological Carbon Storage*, edited by S. Vialle, J. Ajo-Franklin & J. W. Carey, pp. 71-118: American Geophysical Union and John Wiley & Sons, Inc.
- Anovitz, L. M., Cole, D. R., Jackson, A. J., Rother, G., Littrell, K. C., Allard, L. F., Pollington, A. D. & Wesolowski, D. J. (2015). *Geochimica et Cosmochimica Acta* **158**, 199-222.
- Bahadur, J., Melnichenko, Y. B., Mastalerz, M., Furmann, A. & Clarkson, C. R. (2014). *Energy & Fuels* **28**, 6336–6344.
- Bahadur, J., Radlinski, A. P., Melnichenko, Y. B., Mastalerz, M. & Schimmelmann, A. (2015). *Energy & Fuels* **29**, 567-576.
- Bale, H. D. & Schmidt, P. W. (1984). Physical Review Letters 53, 596-599.
- Bevington, P. & Robinson, D. K. (2003). *Data Reduction and Error Analysis for the Physical Sciences*. McGraw-Hill Education.
- Binder, K., Erman, B., Mark, J. E. & Roe, R. J. (2000). *Methods of X-Ray and Neutron Scattering in Polymer Science*. Oxford: Oxford University Press.
- Blach, T., Radlinski, A. P., Edwards, D. S., Boreham, C. J. & Gilbert, E. P. (2020). *International Journal of Coal Geology*, 103495.

- Borsali, R. & Pecora, R. (2008). Soft Matter Characterization. New York, USA: Springer.
- Bressler, I., Kohlbrecher, J. & Thunemann, A. F. (2015). *Journal of Applied Crystallography* 48, 1587-1598.
- Busch, A., Kampman, N., Bertier, P., Pipich, V., Feoktystov, A., Rother, G., Harrington, J., Leu, L., Aertens, M. & Jacops, E. (2018). *Water Resources Research* **54**, 7076–7091.
- Busch, A., Schweinar, K., Kampman, N., Coorn, A., Pipich, V., Feoktystov, A., Leu, L., Amann-Hildenbrand, A. & Bertier, P. (2017). *Geological Society, London, Special Publications* **454**.
- Chacón, P., Morán, F., Díaz, J. F., Pantos, E. & Andreu, J. M. (1998). Biophys J 74, 2760-2775.
- Clarkson, C. R., Freeman, M., He, L., Agamalian, M., Melnichenko, Y. B., Mastalerz, M., Bustin, R. M., Radlinski, A. P. & Blach, T. P. (2012). *Fuel* **95**, 371-385.
- Dewhurst, C. (2002). GRASP software package.
- Feigin, L. A. & Svergun, D. I. (1987). *Structure Analysis by Small-Angle X-ray and Neutron Scattering*. New York: Plenum Press.
- Forster, S., Apostol, L. & Bras, W. (2010). Journal of Applied Crystallography 43, 639-646.
- Franke, D. & Svergun, D. I. (2009). Journal of Applied Crystallography 42, 342-346.
- Fritzsche, H., Huot, J. & Fruchart, D. (2016). *Neutron Scattering and Other Nuclear Techniques for Hydrogen in Materials*. Switzerland: Springer International Publishing
- Guinier, A. & Fournet, G. (1955). Small Angle Scattering of X-rays. New York: John Wiley.
- Hammersley, A. P. (1995). ESRF Internal Report Exp/AH/95-01, FIT2D V5.18 Ref. Manual. Grenoble, France.
- Heenan, R. K. (1999). FISH, program for peak analysis.
- Heenan, R. K., Penfold, J. & King, S. M. (1997). Journal of Applied Crystallography 30, 1140-1147.
- Hinde, A. (2004). Journal of Applied Crystallography 37, 1020-1024.
- Hiragi, Y., Sano, Y. & Matsumoto, T. (2003). Journal of Synchrotron Radiation 10, 193-196.
- Hofmann, A. & Whitten, A. E. (2014). Journal of Applied Crystallography 47, 810-815.
- Homan, E., Konijnenburg, M., Ferrero, C., Ghosh, R. E., Dolbnya, I. P. & Bras, W. (2001). *Journal of Applied Crystallography* **34**, 519-522.
- Hopkins, J. B., Gillilan, R. E. & Skou, S. (2017). Journal of Applied Crystallography 50, 1545-1553.
- Ilavsky, J. & Jemian, P. R. (2009). Journal of Applied Crystallography 42, 347-353.
- Keiderling, U. (1997). Physica B: Condensed Matter 234-236, 1111-1113.
- Konarev, P. V., Petoukhov, M. V., Volkov, V. V. & Svergun, D. I. (2006). *Journal of Applied Crystallography* **39**, 277–286.
- Leu, L., Georgiadis, A., Blunt, M. J., Busch, A., Bertier, P., Schweinar, K., Liebi, M., Menzel, A. & Ott, H. (2016). *Energy & Fuels* **30**, 10282-10297.
- Liu, H., Hexemer, A. & Zwart, P. H. (2012). Journal of Applied Crystallography 45, 587-593.
- Mandelbrot, B. B. (1983). *The fractal geometry of nature*. New York: W. H. Freeman and Company.
- Mares, T. E., Radliński, A. P., Moore, T. A., Cookson, D., Thiyagarajan, P., Ilavsky, J. & Klepp, J. (2012). *International Journal of Coal Geology* **94**, 173-181.
- Mastalerz, M., He, L., Melnichenko, Y. B. & Rupp, J. A. (2012). Energy and Fuels 26, 5109-5120.
- Melnichenko, Y. B. (2015). Small-Angle Scattering from Confined and Interfacial Fluids: Applications to Energy Storage and Environmental Science. TN, USA: Springer.
- Melnichenko, Y. B., He, L., Sakurovs, R., Kholodenko, A. L., Blach, T., Mastalerz, M., Radlinski, A. P., Cheng, G. & Mildner, D. F. R. (2012). *Fuel* **91**, 200–208.
- Meyer, K. & Klobes, P. (1999). Fresenius' Journal of Analytical Chemistry 363, 174-178.
- Muthig, M., Prevost, S., Orglmeister, R. & Gradzielski, M. (2013). *Journal of Applied Crystallography* **46**, 1187-1195.
- Nielsen, S. S., Toft, K. N., Snakenborg, D., Jeppesen, M. G., Jacobsen, J. K., Vestergaard, B., Kutter, J. P. & Arleth, L. (2009). *Journal of Applied Crystallography* **42**, 959-964.
- Petoukhov, M. V., Franke, D., Shkumatov, A. V., Tria, G., Kikhney, A. G., Gajda, M., Gorba, C., Mertens, H. D. T., Konarev, P. V. & Svergun, D. I. (2012). *Journal of Applied Crystallography* **45**, 342-350.
- Porod, G. (1951). Kolloid-Zeitschrift 124, 83-114.
- Porod, G. (1952). Kolloid-Zeitschrift 125, 51-57.
- Radlinski, A. P. (2006). Reviews in Mineralogy and Geochemistry 63, 363-397.

- Radlinski, A. P., Boreham, C. J., Lindner, P., Randl, O., Wignall, G. D., Hinde, A. & Hope, J. M. (2000). *Organic Geochemistry* **31**, 1-14.
- Radlinski, A. P., Busbridge, T. L., Gray, E. M. A., Blach, T. P. & Cookson, D. J. (2009). *International Journal of Coal Geology* 77, 80-89.
- Radlinski, A. P., Ioannidis, M. A., Hinde, A. L., Hainbuchner, M., Baron, M., Rauch, H. & Kline, R. (2002). *Proceedings of 2002 International Symposium of the Society of Core Analysts (SCA2002-35)*. Monterey, California.
- Radlinski, A. P., Ioannidis, M. A., Hinde, A. L., Hainbuchner, M., Baron, M., Rauch, H. & Kline, S. R. (2004). *Journal of Colloid and Interface Science* **274**, 607-612.
- Radlinski, A. P., Mastalerz, M., Hinde, A. L., Hainbuchner, M., Rauch, H., Baron, M., Lin, J. S., Fan, L. & Thiyagarajan, P. (2004). *International Journal of Coal Geology* **59**, 245-271.
- Rezaeyan, A., Pipich, V., Bertier, P., Seemann, T., Leu, L., Kampman, N., Feoktystov, A., Barnsley, L. C. & Busch, A. (2019a). Microstructural Investigation of Mudrock Seals Using Nanometer-Scale Resolution Techniques, Sixth EAGE Shale Workshop, Bordeaux, France: EAGE.
- Rezaeyan, A., Pipich, V., Bertier, P., Seemann, T., Leu, L., Kampman, N., Feoktystov, A., Barnsley, L. C. & Busch, A. (2019b). Quantitative Analysis of the Pore Structure of Premature-To-Postmature Organic Rich Mudrocks Using Small Angle Neutron Scattering, Sixth EAGE Shale Workshop, Bordeaux, France: EAGE.
- Rezaeyan, A., Seemann, T., Bertier, P., Pipich, V., Leu, L., Kampman, N., Feoktystov, A., Barnsley, L. & Busch, A. (2019). Understanding Pore Structure of Mudrocks and Pore-Size Dependent Sorption Mechanism Using Small Angle Neutron Scattering, SPE/AAPG/SEG Asia Pacific Unconventional Resources Technology Conference, p. 13. Brisbane, Australia: Unconventional Resources Technology Conference.
- Sakurovs, R., Koval, L., Grigore, M., Sokolova, A., Ruppert, L. F. & Melnichenko, Y. B. (2018). *International Journal of Coal Geology* **186**, 126-134.
- Schmidt, P. (1982). Journal of Applied Crystallography 15, 567-569.
- Schrank, C. E., Gioseffi, K., Blach, T., Gaede, O., Hawley, A., Milsch, H., Regenauer-Lieb, K. & Radlinski, A. P. (2020). *Journal of Petrology*.
- Seemann, T., Bertier, P., Maes, N., Rezaeyan, A., Pipich, V., Barnsley, L., Busch, A. & Cnudde, V. (2019). 2019, 1-5.
- Vishal, V., Chandra, D., Bahadur, J., Sen, D., Hazra, B., Mahanta, B. & Mani, D. (2019). *Energy & Fuels* **33**, 4835–4848.
- Walther, D., Cohen, F. E. & Doniach, S. (2000). Journal of Applied Crystallography 33, 350-363.
- Zemb, T. & Lindner, P. (2002). *Neutron, X-rays and Light. Scattering Methods Applied to Soft Condensed Matter* North Holland: North-Holland Delta Series.
- Zhao, J. (2011). Journal of Applied Crystallography 44, 1277-1280.